



# Global $\Lambda$ polarization in heavy-ion collisions from a transport model

Hui Li,<sup>1,\*</sup> Long-Gang Pang,<sup>2,†</sup> Qun Wang,<sup>1,‡</sup> and Xiao-Liang Xia<sup>1,§</sup>

<sup>1</sup>*Department of Modern Physics, University of Science and Technology of China, Hefei, Anhui 230026, China*

<sup>2</sup>*Frankfurt Institute for Advanced Studies, Ruth-Moufang-Strasse 1, 60438 Frankfurt am Main, Germany*

(Received 7 April 2017; published 29 November 2017)

The polarizations of  $\Lambda$  and  $\bar{\Lambda}$  hyperons are important quantities in extracting the fluid vorticity of the strongly coupled quark gluon plasma and the magnitude of the magnetic field created in off-central heavy-ion collisions, through the spin-vorticity and spin-magnetic coupling. We computed the energy dependence of the global  $\Lambda$  polarization in off-central Au+Au collisions in the energy range  $\sqrt{s_{NN}} = 7.7\text{--}200$  GeV using a multiphase transport model. The observed polarizations with two different impact parameters agree quantitatively with recent STAR measurements. The energy dependence of the global  $\Lambda$  polarization is decomposed as energy dependence of the  $\Lambda$  distribution at hadronization and the space-time distribution of the fluid-vorticity field. The visualization of both the  $\Lambda$  distribution and the fluid-vorticity field show a smaller tilt at higher collisional energies, which indicates that the smaller global polarization at higher collisional energies is caused by a smaller angular momentum deposition at midrapidity.

DOI: [10.1103/PhysRevC.96.054908](https://doi.org/10.1103/PhysRevC.96.054908)

## I. INTRODUCTION

In off-central heavy-ion collisions, huge orbital angular momenta of order  $10^3\text{--}10^5\hbar$  are generated. How such orbital angular momenta are distributed in the hot and dense matter is an interesting topic to be investigated. There is an inherent correlation between rotation and particle polarization. The Einstein–de Haas effect [1] demonstrates that a sudden magnetization of the electron spins in a ferromagnetic material leads to a mechanical rotation due to angular momentum conservation. Barnett [2] proved the existence of the reverse process—the rotation of an uncharged body leads to the polarization of atoms and spontaneous magnetization. It is expected that quarks are also polarized in the rotating quark-gluon plasma (QGP) created in off-central heavy-ion collisions. Liang and Wang first proposed that  $\Lambda$  hyperons can be polarized along the orbital angular momentum of two colliding nucleus [3,4]. Voloshin suggested that such a polarization can even be observed in unpolarized hadron-hadron collisions [5]. Besides the global orbital angular momentum, the local vorticity created by a fast jet going through the QGP also affects the hadron polarization [6]. The polarization density near equilibrium is first computed in the statistical-hydrodynamic model [7–9] and later confirmed in a quantum kinetic approach [10]. Some hydrodynamic calculations quantitatively predicted the global polarization in off-central heavy-ion collisions [11–14]. The fluid vorticity has also been investigated in transport simulations [15,16]. For more studies of the fluid vorticity and  $\Lambda$  polarization, please refer to Refs. [17–24].

Recently STAR measured the global polarization of  $\Lambda$  and  $\bar{\Lambda}$  in off-central Au+Au collisions in the Beam Energy Scan

(BES) program [25]. From the measured polarization, the fluid vorticity of the strongly coupled QGP and the magnitude of the magnetic field created in off-central heavy-ion collisions are extracted for the first time using the spin-vorticity and spin-magnetic coupling. It indicates that the rotational fluid has the largest vorticity, of the order of  $10^{21}\text{ s}^{-1}$ , that ever existed in the universe. So the strongly coupled QGP has an additional extreme feature: it is the fluid with the highest vorticity. The global polarization of hyperons plays an important role in probing the vorticity field of the QGP. Therefore, it is worth to study the inherent correlation between the global polarization and the microscopic vortical structure in detail.

In this paper, we focus on the energy dependence of the vorticity field and global  $\Lambda$  polarization within a multiphase transport (AMPT) model [26] for nuclear-nuclear collisions in the energy range  $\sqrt{s_{NN}} = 7.7\text{--}200$  GeV. The vorticity field profile given by AMPT is used to compute the global polarization of  $\Lambda$  and  $\bar{\Lambda}$  produced in the hadronization stage using the spin-vorticity coupling. The paper is organized as follows. In Sec. II, we give the formula for the polarization induced by vorticity. In Sec. III, we introduce the numerical method we use. The numerical results and discussions are presented in Sec. IV. We finally give a summary in Sec. V.

In this paper, we use the following conventions. The metric tensor is chosen as  $g_{\mu\nu} = \text{diag}(1, -1, -1, -1)$  and the Levi-Civita symbol satisfies  $\epsilon^{0123} = 1$ . The symbols in boldface represent the spatial components of four-vectors, for example,  $S^\mu = (S^0, \mathbf{S})$  denotes the spin four-vector and  $u^\mu = \gamma(1, \mathbf{v})$  denotes the fluid velocity four-vector with  $\gamma = 1/\sqrt{1 - \mathbf{v}^2}$  being the Lorentz factor.

## II. A POLARIZATION FROM VORTICITY

In local thermal equilibrium, the ensemble average of the spin vector for spin-1/2 fermions with four-momentum  $p$  at space-time point  $x$  is obtained from the statistical-hydrodynamical model [9] as well as the Wigner function

\*lihui12@mail.ustc.edu.cn

†pang@fias.uni-frankfurt.de

‡qunwang@ustc.edu.cn

§xiaxl@mail.ustc.edu.cn

approach [10] and reads

$$S^\mu(x, p) = -\frac{1}{8m}(1 - n_F)\epsilon^{\mu\nu\rho\sigma} p_\nu \varpi_{\rho\sigma}(x), \quad (1)$$

where the thermal vorticity tensor is given by

$$\varpi_{\mu\nu} = \frac{1}{2}(\partial_\nu \beta_\mu - \partial_\mu \beta_\nu) \quad (2)$$

with  $\beta^\mu = u^\mu/T$  being the inverse-temperature four-velocity. In Eq. (1),  $m$  is the mass of the particle and  $n_F = 1/[1 + \exp(\beta \cdot p \mp \mu/T)]$  is the Fermi-Dirac distribution function for particles (-) and antiparticles (+).

Some approximations can be made in Eq. (1) to simplify the computation of the global  $\Lambda$  polarization. Since the temperature at hadronization is much lower than the mass of the  $\Lambda$ , the number density of  $\Lambda$ 's is very small so that we can make the approximation  $1 - n_F \simeq 1$  as in Ref. [11]. With this approximation, Eq. (1) is the same for  $\Lambda$  and  $\bar{\Lambda}$ . Care has to be taken since a finite chemical potential in  $n_F$  or spin-magnetic coupling could induce a difference between  $\Lambda$  and  $\bar{\Lambda}$ . However, the difference between the polarizations of  $\Lambda$  and  $\bar{\Lambda}$  measured in the STAR experiment is not distinguishable within errors [25,27]. For simplicity, we also do not distinguish  $\Lambda$  and  $\bar{\Lambda}$  in the present research. Therefore, Eq. (1) is rewritten as

$$S^\mu(x, p) = -\frac{1}{8m}\epsilon^{\mu\nu\rho\sigma} p_\nu \varpi_{\rho\sigma}(x). \quad (3)$$

By decomposing the thermal vorticity in Eq. (2) into the following components:

$$\begin{aligned} \varpi_T &= (\varpi_{0x}, \varpi_{0y}, \varpi_{0z}) = \frac{1}{2} \left[ \nabla \left( \frac{\gamma}{T} \right) + \partial_t \left( \frac{\gamma \mathbf{v}}{T} \right) \right], \\ \varpi_S &= (\varpi_{yz}, \varpi_{zx}, \varpi_{xy}) = \frac{1}{2} \nabla \times \left( \frac{\gamma \mathbf{v}}{T} \right), \end{aligned} \quad (4)$$

Eq. (3) can be rewritten as

$$\begin{aligned} S^0(x, p) &= \frac{1}{4m} \mathbf{p} \cdot \varpi_S, \\ \mathbf{S}(x, p) &= \frac{1}{4m} (E_p \varpi_S + \mathbf{p} \times \varpi_T), \end{aligned} \quad (5)$$

where  $E_p$ ,  $\mathbf{p}$ ,  $m$  are the  $\Lambda$ 's energy, momentum, and mass, respectively.

The spin vector in Eq. (5) is defined in the center of mass (c.m.) frame of Au+Au collisions. In the STAR experiment, the  $\Lambda$  polarization is measured in the local rest frame of the  $\Lambda$  by its decay proton's momentum. The spin vector of  $\Lambda$  in its rest frame is denoted as  $S^{*\mu} = (0, \mathbf{S}^*)$  and is related to the same quantity in the c.m. frame by a Lorentz boost

$$\mathbf{S}^*(x, p) = \mathbf{S} - \frac{\mathbf{p} \cdot \mathbf{S}}{E_p(m + E_p)} \mathbf{p}. \quad (6)$$

By taking the average of  $\mathbf{S}^*$  over all  $\Lambda$  particles produced at the hadronization stage of AMPT, we obtain the average spin vector

$$\langle \mathbf{S}^* \rangle = \frac{1}{N} \sum_{i=1}^N \mathbf{S}^*(x_i, p_i), \quad (7)$$

where  $N$  is the number of  $\Lambda$ s in all events and  $i$  labels one individual  $\Lambda$ . The global  $\Lambda$  polarization in the STAR

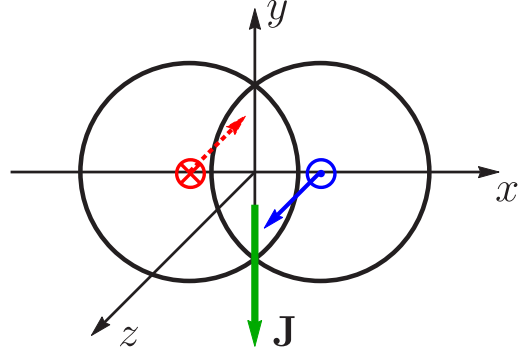


FIG. 1. Schematic picture of an off-central collision.

experiment is the projection of  $\langle \mathbf{S}^* \rangle$  onto the direction of global angular momentum in off-central collisions (normal to the reaction plane),

$$P = 2 \frac{\langle \mathbf{S}^* \rangle \cdot \mathbf{J}}{|\mathbf{J}|}, \quad (8)$$

where we have included a normalization factor ( $P$  is normalized to 1) and  $\mathbf{J}$  denotes the global orbital angular momentum of off-central collisions.

### III. MODEL SETUP

The string-melting version of the AMPT model is employed as event generator. It contains four stages: the initial condition, a parton cascade, hadronization, and hadronic rescatterings. In this paper, we coarse-grain the parton stage to calculate the thermal vorticity, and collect  $\Lambda$  hyperons produced in the hadronization stage for calculating the global polarization. Some notations are made as follows. The reaction plane is fixed to be the  $x$ - $z$  plane where  $x$  is the direction of impact parameter  $\mathbf{b}$  and  $z$  is the beam direction as shown in Fig. 1. In off-central collisions, one nucleus centered at  $(x = b/2, y = 0)$  in the transverse plane moves along the  $z$  direction, while the other nucleus centered at  $(x = -b/2, y = 0)$  moves along the  $-z$  direction, with  $b \equiv |\mathbf{b}|$ . The total angular momentum  $\mathbf{J}$  of the system and the average spin vector  $\langle \mathbf{S}^* \rangle$  thus point along the  $-y$  direction. However, the  $y$  component of the local thermal vorticity  $\varpi_S$  ( $\varpi_{zx}$ ) is not forced to be negative everywhere in the fireball. In fact the local vorticity is a measure of local rotation in the comoving frame of one cell. Both relativistic fluid dynamics and transport models exhibit rich local vorticity structures [15–20,23,24]. The global angular momentum is the integral of local vorticity over all regions.

The AMPT model tracks the positions and momenta of all particles at any given time. These particles need to be fluidized on space-time grids in order to calculate the velocity field numerically [15,16,28]. In the present study, the space-time volume of the system is divided into 30 time steps with the interval  $\Delta t = 1$  fm/c,  $41 \times 41$  cells in transverse plane with spacing  $\Delta x = \Delta y = 0.5$  fm, and 21 cells in the rapidity direction of size  $\Delta \eta = 0.5$  unit. Each cell is labeled by its time  $t$  and the coordinate of its center  $(x, y, z)$ . The thermal vorticity  $\varpi_{\mu\nu}$  in each space-time cell is constructed by the following method. We first calculate the energy-momentum tensor  $T^{\mu\nu}$

in each cell by computing the sum of  $p^\mu p^\nu / E$  of all particles in the cell and taking an average over many events,

$$T^{\mu\nu}(t,x,y,z) = \frac{1}{N_e \Delta V} \sum_i \sum_j \frac{p_{ij}^\mu p_{ij}^\nu}{E_{ij}}, \quad (9)$$

where  $p_{ij}^\mu = (E_{ij}, \mathbf{p}_{ij})$  denotes the  $j$ th particle's four-momentum in a certain cell in the  $i$ th event,  $\Delta V$  represents the volume of the cell, and  $N_e$  is the number of events. Then the four-velocity  $u^\mu$  as well as the energy density  $\varepsilon$  in each cell are obtained by solving the eigenvalue problem  $T^{\mu\nu} u_\nu = \varepsilon u^\mu$ , where  $u^\mu$  is normalized by  $u^\mu u_\mu = 1$ . The temperature field  $T$  is determined from  $\varepsilon$  using the equation of state  $\varepsilon(T)$  in lattice QCD [29,30]. Finally, the obtained velocity field and temperature field are used to calculate the thermal vorticity for each cell following Eq. (2), using the finite-difference method (FDM).

For each BES energy and our chosen impact parameter (7 and 9 fm), we generate  $10^5$  events and take the event average in Eq. (9) over them. In this way, the event-by-event fluctuation of the velocity is removed, so some event-by-event structures of the fluid, such as vortex pairings in the transverse plane due to hot spots [20] are wiped out. However, this is not a problem for the current study on the global  $\Lambda$  polarization since it is an integral effect of all regions and the local fluctuations are canceled or smeared when taking the sum over contributions.

Once the thermal vorticity field is stored in the four-dimensional space-time cells, the spin vector of a  $\Lambda$  hyperon can be computed from the spin-vorticity coupling as given in Eq. (5), using the value of the local thermal vorticity in the cell where and when the  $\Lambda$  is produced. Then the global  $\Lambda$  polarization is obtained by taking average over the spin vectors of all  $\Lambda$  hyperons by Eq. (7) and is projected on the angular momentum direction by Eq. (8). For each chosen energy and impact parameter, about  $2 \times 10^6$   $\Lambda$  hyperons are used to take the average.

## IV. RESULTS AND DISCUSSIONS

### A. Results for the $\Lambda$ polarization

We run simulations at BES energies  $\sqrt{s_{NN}} = 7.7, 11.5, 14.5, 19.6, 27, 39, 62.4,$  and  $200$  GeV. For each energy, we choose two fixed impact parameters  $b = 7$  fm and  $9$  fm from the range  $b = 5.5$ – $11.3$  fm corresponding to the 20%–50% centrality class of the STAR experiment [31]. To match the Time Projection Chamber (TPC) region in the STAR experiment [25],  $\Lambda$  hyperons are selected from the midrapidity region  $|\eta| < 1$ . We calculate the global  $\Lambda$  polarization using the method described in Sec. III. The results are shown in Fig. 2.

As shown in Fig. 2, the global polarization is largest at  $\sqrt{s_{NN}} = 7.7$  GeV and decreases as the collisional energy increases. It almost vanishes at  $\sqrt{s_{NN}} = 200$  GeV. The global polarization at  $b = 9$  fm is larger than that at  $b = 7$  fm at a specific energy. This is consistent with previous studies where the averaged and weighted vorticity increases with the impact parameter in the range  $b < 10$  fm [15,16]. The results shown in Fig. 2 only contain primary  $\Lambda$  hyperons that are directly produced at hadronization.

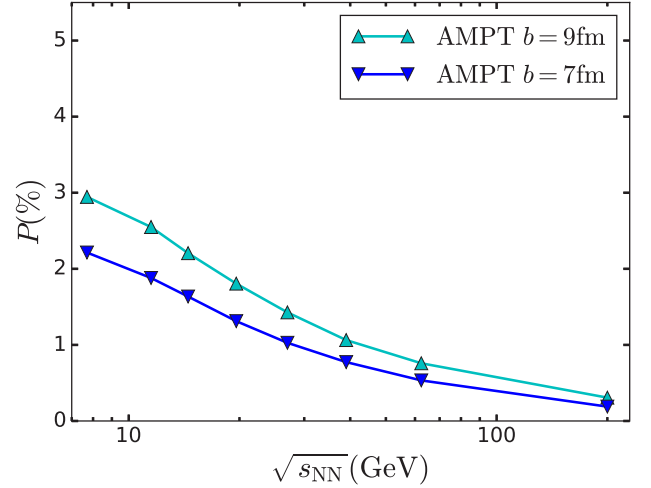


FIG. 2. The global  $\Lambda$  polarization at two impact parameters  $b = 7$  fm (the blue lower line) and  $9$  fm (the cyan upper line).

In practice, some  $\Lambda$  hyperons are secondary particles produced from resonance decays, like  $\Sigma(1385) \rightarrow \Lambda + \pi$  (strong decay) or  $\Sigma^0 \rightarrow \Lambda + \gamma$  (electromagnetic decay). It was shown in Ref. [32] that including feed-down  $\Lambda$ s decreases the global polarization. Different decay channels or decay parameters give different suppression factors. For direct decays and two-step cascade decays, the global polarization is estimated to be suppressed by about 17%, using the contributions to  $\Lambda$  from Ref. [31] and the decay branching ratios from Ref. [33]. For comparison, the suppression ratio is estimated to be 15% in Ref. [12] and 20% in Ref. [32].

In Fig. 3, we compare our results with the STAR data. The solid line represents the global polarization of primary  $\Lambda$ s from the average over two impact parameters. Primary plus feed-down  $\Lambda$ s result in a suppression of 17%, as shown by the

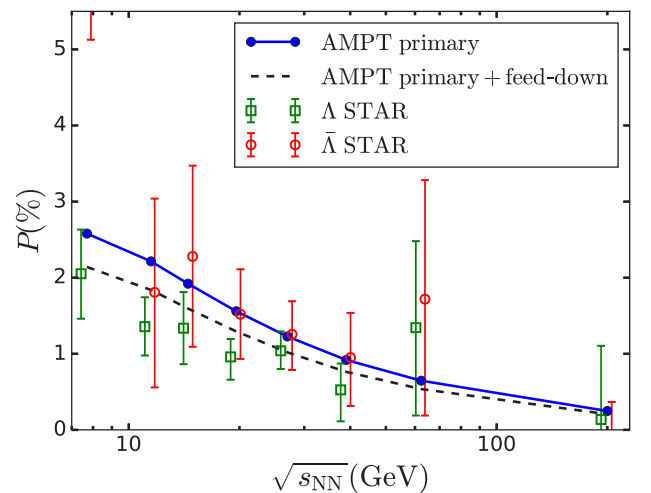


FIG. 3. The global  $\Lambda$  polarization at energies from 7.7 GeV to 200 GeV. The blue solid line represents the global polarization of primary  $\Lambda$ s and the black dashed line shows global polarization of primary plus feed-down  $\Lambda$ s. The unfilled squares and circles represent the global  $\Lambda$  and  $\bar{\Lambda}$  polarization measurements at STAR [25,34].

dashed line, which is closer to the data than the one for primary  $\Lambda$ s only. The splitting between  $\Lambda$  and  $\bar{\Lambda}$  is not included in the current study.

### B. Collisional energy dependence of global polarization

As shown in last subsection, the global  $\Lambda$  polarization decreases as the collisional energy increases: the value of  $P$  at 7.7 GeV is more than 10 times of that at 200 GeV. This behavior contradicts the energy dependence of the global angular momentum. The reason for a small global polarization at high collisional energy where angular momentum is large is investigated in this section.

According to our numerical calculation, we find the most contribution to the global  $\Lambda$  polarization comes from the  $\varpi_S$  term in Eq. (5) rather than the  $\varpi_T$  term. Similar result can also be found in Ref. [12]. Therefore the global polarization in Eq. (8) can be approximated as

$$P = \frac{1}{N} \sum_{i=1}^N \frac{C}{2} \varpi_{zx}(x_i), \quad (10)$$

where  $\varpi_{zx}(x_i)$  is the  $y$  component of  $\varpi_S$  in Eq. (4) at the space-time point of the  $i$ th  $\Lambda$ , and the coefficient  $C$  encapsulates the contribution from the ratio  $E_p/m$  in Eq. (5) and the Lorentz boost correction from  $\mathbf{S}$  to  $\mathbf{S}^*$  in Eq. (6). In the nonrelativistic limit,  $\Lambda$ 's energy-momentum ( $E_p, \mathbf{p}$ ) tends to  $(m, 0)$  which leads to  $C = 1$ , so one can treat the coefficient  $C$  as a relativistic correction. By comparing the global polarization calculated from Eqs. (5)–(8) with the one from Eq. (10), we find  $C$  is around 1 which is not sensitive to the collisional energy. Then the energy behavior of the polarization is approximately proportional to the rest part of Eq. (10), which we can rewrite in an integration form

$$P \propto \int d^4x f_\Lambda(x) \varpi_{zx}(x), \quad (11)$$

where we have omitted the coefficient  $C/2$ , and  $f_\Lambda(x)$  is the space-time distribution of  $\Lambda$  at hadronization. One can see clearly from Eq. (11) that the global polarization is jointly determined by the space-time distribution of  $\Lambda$  and the thermal vorticity field  $\varpi_{zx}$ .

In the following, we investigate the energy dependence of  $f_\Lambda$  and  $\varpi_{zx}$  and study how they combine to determine the energy behavior of the polarization. We show  $f_\Lambda$  and  $\varpi_{zx}$  in Figs. 4 and 5 separately for  $\sqrt{s_{NN}} = 7.7$  GeV and 200 GeV. The results at other BES energies between these two energies can be regarded as some kind of interpolation between them. We also select  $b = 7$  fm for illustration.

Figure 4 shows the distribution of the  $\Lambda$ 's production position integrated over  $t$  and  $y$ , so it is a function of  $x$  and the space-time rapidity  $\eta$ . We see that  $f_\Lambda$  has a sideways tilt, namely more  $\Lambda$  are produced in the upper-right and lower-left region due to an asymmetric matter density distribution in off-central collisions. In the midrapidity region  $|\eta| < 1$  (between the black dashed lines in Fig. 4) that we are interested in,  $f_\Lambda$  still shows a tilt at 7.7 GeV, but it is almost symmetric in both  $x$  and  $\eta$  at 200 GeV. The latter is the result of a broader rapidity

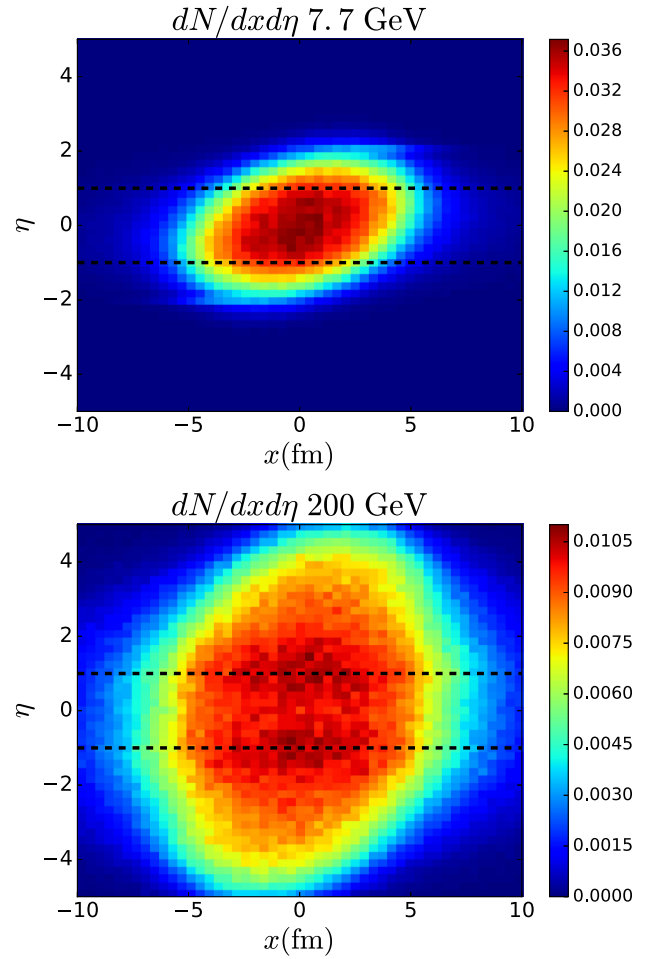


FIG. 4. The distribution of the  $\Lambda$ 's production position integrated over  $t$  and  $y$  as a function of  $x$  and  $\eta$  at  $\sqrt{s_{NN}} = 7.7$  GeV (upper panel) and 200 GeV (lower panel). The midrapidity region  $|\eta| < 1$  is between the black dashed lines.

range over which the fireball extends at higher energies so that the tilt can only be observed at large rapidity.

Figure 5 shows the spatial distribution of  $\varpi_{zx}$  on the reaction plane ( $y = 0$ ), in which we take  $t = 5$  fm/c as an example for illustration. Here  $\varpi_{zx}$  is not weighted by the particle number or energy density. We can see the thermal vorticity field  $\varpi_{zx}$  shows a quadrupole structure, i.e., it has opposite signs on different sides of each axis. Similar patterns are also found in other models or simulations [15,19,23,24]. At 200 GeV the thermal vorticity field  $\varpi_{zx}$  is nearly a perfectly odd function of both  $x$  and  $\eta$ . This structure can be understood by the radial flow of the system, in which the transverse velocity  $v_x$  is an odd function of  $x$  but an even function of  $\eta$  [15]. At 7.7 GeV the thermal vorticity field  $\varpi_{zx}$  is not an odd function as evidenced by the fact that  $\varpi_{zx}$  is nonvanishing in the central region  $x \simeq 0$  and  $\eta \simeq 0$ . We also see in Fig. 5 that  $\varpi_{zx}$  has the same magnitude at 7.7 and 200 GeV. For the time evolution of  $\varpi_{zx}$ , we have checked the magnitude of  $\varpi_{zx}$  decays with time and the decay rate is not sensitive to the collisional energy. Therefore  $\varpi_{zx}$  at different energies are always at the same magnitude during the time evolution. We also checked that the

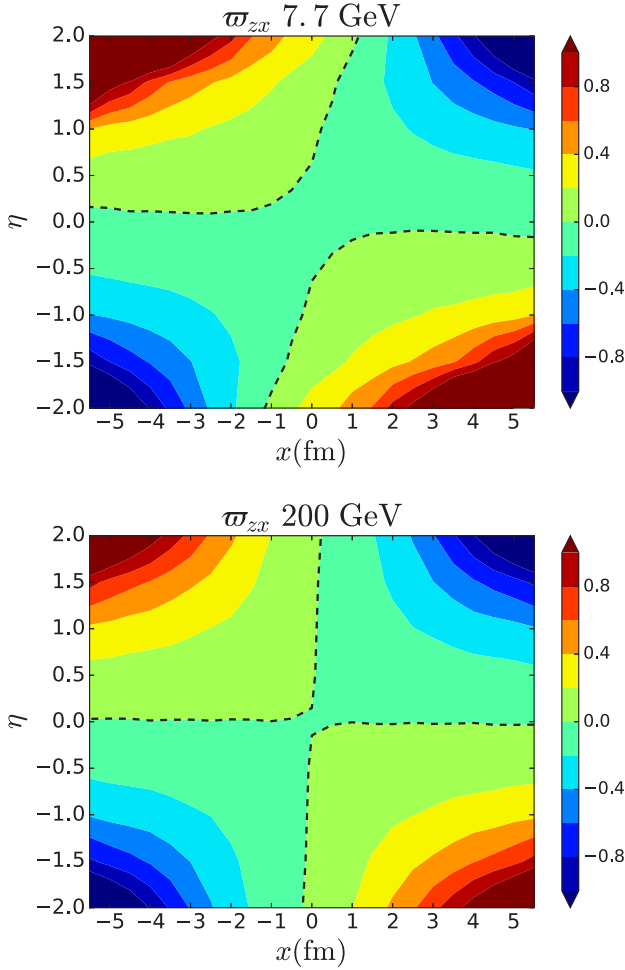


FIG. 5. The thermal vorticity  $\varpi_{zx}$  on the reaction plane ( $y = 0$ ) at  $t = 5 \text{ fm}/c$  at  $\sqrt{s_{NN}} = 7.7 \text{ GeV}$  (upper panel) and  $200 \text{ GeV}$  (lower panel). The black dashed lines represent the contour where  $\varpi_{zx} = 0$ .

pattern of  $\varpi_{zx}$  in spatial distribution does not change with time at each collisional energy.

Given the space-time distribution of  $f_{\Lambda}$  and  $\varpi_{zx}$  at  $7.7$  and  $200 \text{ GeV}$ , we now study how they combine to give the global polarization. We first look at the effect of their spatial distribution. We know that  $\varpi_{zx}$  is negative in the upper-right and lower-left region and leads to a  $\Lambda$  polarization along the  $-y$  direction, and  $\varpi_{zx}$  is positive in the upper-left and lower-right region and gives a  $\Lambda$  polarization along the  $+y$  direction. When taking the average, these opposite polarizations cancel each other. Therefore the global polarization depends on how many  $\Lambda$  hyperons are produced in the positive and negative-vorticity region.

At  $200 \text{ GeV}$ , as shown in Figs. 4 and 5,  $\varpi_{zx}$  ( $f_{\Lambda}$ ) is nearly a perfectly odd (even) function in both  $x$  and  $\eta$  in the midrapidity region. There is almost an equal number of  $\Lambda$  hyperons produced in the positive and the negative-vorticity region. Therefore the global  $\Lambda$  polarization is almost vanishing at  $200 \text{ GeV}$ . At  $7.7 \text{ GeV}$ , there are more  $\Lambda$  hyperons produced in the negative-vorticity region because: (1)  $\varpi_{zx}$  is negative in the central region ( $x \simeq 0$  and  $\eta \simeq 0$ ); (2) the tilt shape of  $f_{\Lambda}$  leads more  $\Lambda$ s produced in the upper-right and lower-left

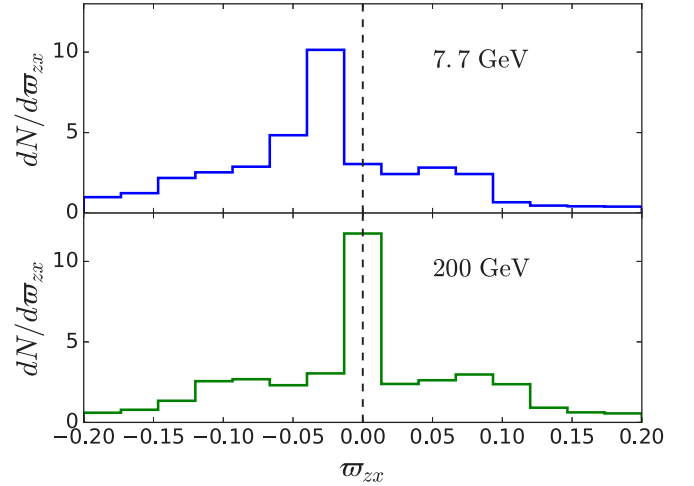


FIG. 6. The distribution of the number of  $\Lambda$  hyperons  $dN/d\varpi_{zx}$ .

region than the upper-left and lower-right region. As the result, the global  $\Lambda$  polarization at  $7.7 \text{ GeV}$  is significantly nonzero.

The above argument is supported by Fig. 6 where we discretize the values of  $\varpi_{zx}$  into several bins and count the number of  $\Lambda$  hyperons produced in the region with the specific  $\varpi_{zx}$  value. The figure clearly shows more  $\Lambda$  hyperons are produced in the negative-vorticity region at  $7.7 \text{ GeV}$ , while an almost equal number of  $\Lambda$  hyperons is produced in both the positive and the negative-vorticity region at  $200 \text{ GeV}$ .

Beside the spatial distribution, the global polarization is also related to when  $\Lambda$  hyperons are produced. Due to the lower temperature of the fireball, the mean  $\Lambda$  production time at  $7.7 \text{ GeV}$  is earlier than that at  $200 \text{ GeV}$ . As  $\varpi_{zx}$  decays with time, when  $\Lambda$  hyperons are produced at  $200 \text{ GeV}$  the magnitude of  $\varpi_{zx}$  is smaller than that at  $7.7 \text{ GeV}$ . This effect also contributes to the energy behavior of the global polarization.

Both angular momentum and global polarization are related to the vorticity. The angular momentum is an integral effect of vorticity weighted by the moment of inertia over the volume of fireball,

$$\mathbf{J} = \int d^3x I(x)\boldsymbol{\omega}(x), \quad (12)$$

where  $I(x)$  is the moment of inertia density of fireball and  $\boldsymbol{\omega} = \nabla \times \mathbf{v}/2$  is the nonrelativistic vorticity. The exact form of  $I(x)$  in fireball is not clear. A well motivated assumption is  $I(x)$  being proportional to the particle number or energy density, see the discussions in [15]. The total amount of the moment of inertia increases with the collisional energy, and so does the total angular momentum of fireball. Such behavior is opposite to the global  $\Lambda$  polarization. However, in the midrapidity region of fireball, the angular momentum should decrease as the collisional energy increases, because  $I(x)$  is nearly symmetric in the positive and the negative-vorticity region at high energy, just like  $f_{\Lambda}(x)$ . In this way, the energy dependence of  $\Lambda$  polarization can be understood by the smaller angular momentum deposited at midrapidity for higher collisional energies. We also note that what happens in the mid-rapidity region at high energy is quite similar to the situation in central

collisions ( $b = 0$ ), in which  $f_\Lambda(x)$  and  $I(x)$  ( $\varpi_{zx}$  and  $\omega_y$ ) are exactly even (odd) functions of  $x$  and  $\eta$ , therefore even though nonzero local vorticity is generated, the total angular momentum and global  $\Lambda$  polarization are vanishing after taking the integral (or average).

## V. SUMMARY

In this paper we calculated the global  $\Lambda$  polarization in Au+Au collisions at BES energies  $\sqrt{s_{NN}} = 7.7\text{--}200$  GeV with the AMPT model. With the feed-down  $\Lambda$  correction from resonance decays, the magnitude of the global polarization increases from about 0.2% to 2.1% as the collisional energy decreases from 200 to 7.7 GeV which agrees with experimental measurements at STAR [25] within the error bars.

To explain this energy behavior, we extracted the dominant contribution to the global polarization as Eq. (11). The global polarization is jointly determined by the space-time distribution of  $\Lambda$  and the thermal vorticity field. The larger

global polarization at lower collisional energies is due to (1) more  $\Lambda$ s are produced in the negative-vorticity region at lower energies due to larger sideways tilt and slower expansion, and (2) earlier  $\Lambda$ s production at lower energies which means the magnitude of vorticity does not decay too much.

## ACKNOWLEDGMENTS

The authors thank Yin Jiang, Jinfeng Liao, Zi-Wei Lin, Michael A. Lisa, Dirk H. Rischke, Zebo Tang, and Zhangbu Xu for helpful discussions. We also thank the anonymous referee for useful comments. H.L., Q.W., and X.L.X. are supported in part by the Major State Basic Research Development Program (973 Program) in China under Grants No. 2015CB856902 and No. 2014CB845402 and by the National Natural Science Foundation of China (NSFC) under Grant No. 11535012. L.G.P. acknowledges funding through the Helmholtz Young Investigator Group VH-NG-822 from the Helmholtz Association and the GSI Helmholtzzentrum für Schwerionenforschung (GSI).

- 
- [1] A. Einstein and W. J. de Haas, *Verh. Dtsch. Phys. Ges.* **17**, 152 (1915).
- [2] S. J. Barnett, *Phys. Rev.* **6**, 239 (1915).
- [3] Z. T. Liang and X. N. Wang, *Phys. Rev. Lett.* **94**, 102301 (2005); **96**, 039901(E) (2006).
- [4] J. H. Gao, S. W. Chen, W. T. Deng, Z. T. Liang, Q. Wang, and X. N. Wang, *Phys. Rev. C* **77**, 044902 (2008).
- [5] S. A. Voloshin, *arXiv:nucl-th/0410089*.
- [6] B. Betz, M. Gyulassy, and G. Torrieri, *Phys. Rev. C* **76**, 044901 (2007).
- [7] F. Becattini, F. Piccinini, and J. Rizzo, *Phys. Rev. C* **77**, 024906 (2008).
- [8] F. Becattini and F. Piccinini, *Ann. Phys. (NY)* **323**, 2452 (2008).
- [9] F. Becattini, V. Chandra, L. Del Zanna, and E. Grossi, *Ann. Phys. (NY)* **338**, 32 (2013).
- [10] R. H. Fang, L. G. Pang, Q. Wang, and X. N. Wang, *Phys. Rev. C* **94**, 024904 (2016).
- [11] F. Becattini, L. P. Csernai, and D. J. Wang, *Phys. Rev. C* **88**, 034905 (2013); F. Becattini, L. P. Csernai, D. J. Wang, and Y. L. Xie, *ibid.* **93**, 069901(E) (2016).
- [12] I. Karpenko and F. Becattini, *Eur. Phys. J. C* **77**, 213 (2017).
- [13] Y. L. Xie, M. Bleicher, H. Stocker, D. J. Wang, and L. P. Csernai, *Phys. Rev. C* **94**, 054907 (2016).
- [14] Y. Xie, D. Wang, and L. P. Csernai, *Phys. Rev. C* **95**, 031901(R) (2017).
- [15] Y. Jiang, Z. W. Lin, and J. Liao, *Phys. Rev. C* **94**, 044910 (2016); **95**, 049904(E) (2017).
- [16] W. T. Deng and X. G. Huang, *Phys. Rev. C* **93**, 064907 (2016).
- [17] L. P. Csernai, V. K. Magas, and D. J. Wang, *Phys. Rev. C* **87**, 034906 (2013).
- [18] L. P. Csernai, D. J. Wang, M. Bleicher, and H. Stöcker, *Phys. Rev. C* **90**, 021904(R) (2014).
- [19] F. Becattini *et al.*, *Eur. Phys. J. C* **75**, 406 (2015).
- [20] L. G. Pang, H. Petersen, Q. Wang, and X. N. Wang, *Phys. Rev. Lett.* **117**, 192301 (2016).
- [21] A. Aristova, D. Frenklakh, A. Gorsky, and D. Kharzeev, *J. High Energy Phys.* **10** (2016) 029.
- [22] M. Baznat, K. Gudima, A. Sorin, and O. Teryaev, *Phys. Rev. C* **88**, 061901(R) (2013).
- [23] O. Teryaev and R. Usubov, *Phys. Rev. C* **92**, 014906 (2015).
- [24] Y. B. Ivanov and A. A. Soldatov, *Phys. Rev. C* **95**, 054915 (2017).
- [25] L. Adamczyk *et al.* (STAR Collaboration), *Nature* **548**, 62 (2017).
- [26] Z. W. Lin, C. M. Ko, B. A. Li, B. Zhang, and S. Pal, *Phys. Rev. C* **72**, 064901 (2005).
- [27] I. Upsal for the STAR Collaboration, talk given at Quark Matter 2017.
- [28] D. Oliinychenko and H. Petersen, *Phys. Rev. C* **93**, 034905 (2016).
- [29] S. Borsanyi, G. Endrodi, Z. Fodor, S. D. Katz, S. Krieg, C. Ratti, and K. K. Szabo, *J. High Energy Phys.* **08** (2012) 053.
- [30] A. Bazavov, H. T. Ding, P. Hegde, O. Kaczmarek, F. Karsch, E. Laermann, Y. Maezawa, S. Mukherjee, H. Ohno, P. Petreczky, H. Sandmeyer, P. Steinbrecher, C. Schmidt, S. Sharma, W. Soeldner, and M. Wagner, *Phys. Rev. D* **95**, 054504 (2017).
- [31] Z. Qiu, *arXiv:1308.2182* [nucl-th].
- [32] F. Becattini, I. Karpenko, M. A. Lisa, I. Upsal, and S. A. Voloshin, *Phys. Rev. C* **95**, 054902 (2017).
- [33] K. A. Olive *et al.* (Particle Data Group), *Chin. Phys. C* **38**, 090001 (2014).
- [34] B. I. Abelev *et al.*, (STAR Collaboration), *Phys. Rev. C* **76**, 024915 (2007); **95**, 039906(E) (2017).